Title

Rupture speed dependence on initial stress profiles: Insights from glacier and laboratory stick-slip

Journal

Earth and Planetary Science Letters, 411

ISSN

0012-821X

Authors

Walter, JI
Svetlizky, I
Fineberg, J
et al.

Publication Date

2015-02-01

DOI

10.1016/j.epsl.2014.11.025

Peer reviewed

Earth and Planetary Science Letters 411 (2015) 112–120

Contents lists available at ScienceDirect

Earth and Planetary Science Letters

www.elsevier.com/locate/epsl

Rupture speed dependence on initial stress profiles: Insights from glacier and laboratory stick-slip

Jacob I. Walter [a,*], Ilya Svetlizky [b], Jay Fineberg [b], Emily E. Brodsky [c], Slawek Tulaczyk [c], C. Grace Barcheck [c], Sasha P. Carter [d]

[a] Institute for Geophysics, University of Texas at Austin, Unites States
[b] Racah Institute of Physics, The Hebrew University of Jerusalem, Israel
[c] Department of Earth and Planetary Sciences, University of California, Santa Cruz, United States
[d] Scripps Institution of Oceanography, University of California, San Diego, United States

ARTICLE INFO

Article history:
Received 3 April 2014
Received in revised form 23 October 2014
Accepted 4 November 2014
Available online 18 December 2014
Editor: J. Brodholt

Keywords:
frictional stick-slip
ice sheet motion
earthquake physics
slow slip
ice streams

ABSTRACT

Slow slip events are now well-established in fault and glacier systems, though the processes controlling slow rupture remain poorly understood. The Whillans Ice Plain provides a window into these processes through bi-daily stick-slip seismic events that displace an ice mass over 100 km long with a variety of rupture speeds observed at a single location. We compare the glacier events with laboratory experiments that have analogous loading conditions. Both systems exhibit average rupture velocities that increase systematically with the pre-rupture stresses, with local rupture velocities exhibiting large variability that correlates well with local interfacial stresses. The slip events in both cases are not time-predictable, but clearly slip-predictable. Local pre-stress may control rupture behavior in a range of frictional failure events, including earthquakes.

1. Introduction

The physical controls on rupture and slip velocities are a persistent and perplexing issue in rupture mechanics. Once a crack exceeds a critical length, it generally accelerates to the dynamically limited Rayleigh wave velocity, which is between 90 and 95% of the shear wave velocity. While exceedingly difficult to measure during natural slip events, like earthquakes, many events rupture at an average rate that can approach and sometimes surpass the shear wave speed of the rocks through which they propagate (Kanamori and Brodsky, 2004). However, since the discovery of slow slip events over a decade ago, we now also understand that faults can fail with rupture velocities significantly below shear wave velocity and slip velocities that only exceed the long-term plate motion by an order of magnitude (Dragert et al., 2001; Peng and Gomberg, 2010; Beroza and Ide, 2011). Glaciers can also slip in transient events that can have rupture velocities ~10% of the local shear wave velocity and slip velocities an order of magnitude above the long-term slip velocities (Wiens et al., 2008; Winberry et al., 2009). For this new class of slow-slip events, the question remains what controls the rupture and slip velocities.

The case of Whillans Ice Plain, Antarctica, is particularly important in the study of slow rupture as this natural system produces frequent, large, and well-documented slip events. Each day, as many as two slip events occur beneath the Whillans Ice Plain over a region ~100 km long (Fig. 1) (Bindschadler et al., 2003; Wiens et al., 2008; Winberry et al., 2009, 2011; Walter et al., 2011). During periods between fast slip events, the ice flows downhill at a steady rate of less than 0.001 m/min, then suddenly increases its speed by more than an order of magnitude at tidal periods, slipping up to ~0.5 m in ~30 min. Individual rupture fronts propagate with average velocities on the order of ~100 m/s (Wiens et al., 2008) from two distinct nucleation regions that vary with the tide (Winberry et al., 2009; Pratt et al., 2014).

Early work attributed the anomalously low rupture velocity of the Whillans events to the low local shear wave velocity of till (Bindschadler et al., 2003). Surprisingly, more recent studies have established that the rupture velocity varies systematically with loading over the tidal cycle and therefore cannot be controlled solely by the material properties (Wiens et al., 2008). Total slip, recurrence time and nucleation location also co-vary with rupture velocity and the tidal cycle (Winberry et al., 2009; Walter et al., 2011; Winberry et al., 2011).

* Corresponding author.
E-mail address: jakeiwalter@gmail.com (J.I. Walter).

http://dx.doi.org/10.1016/j.epsl.2014.11.025

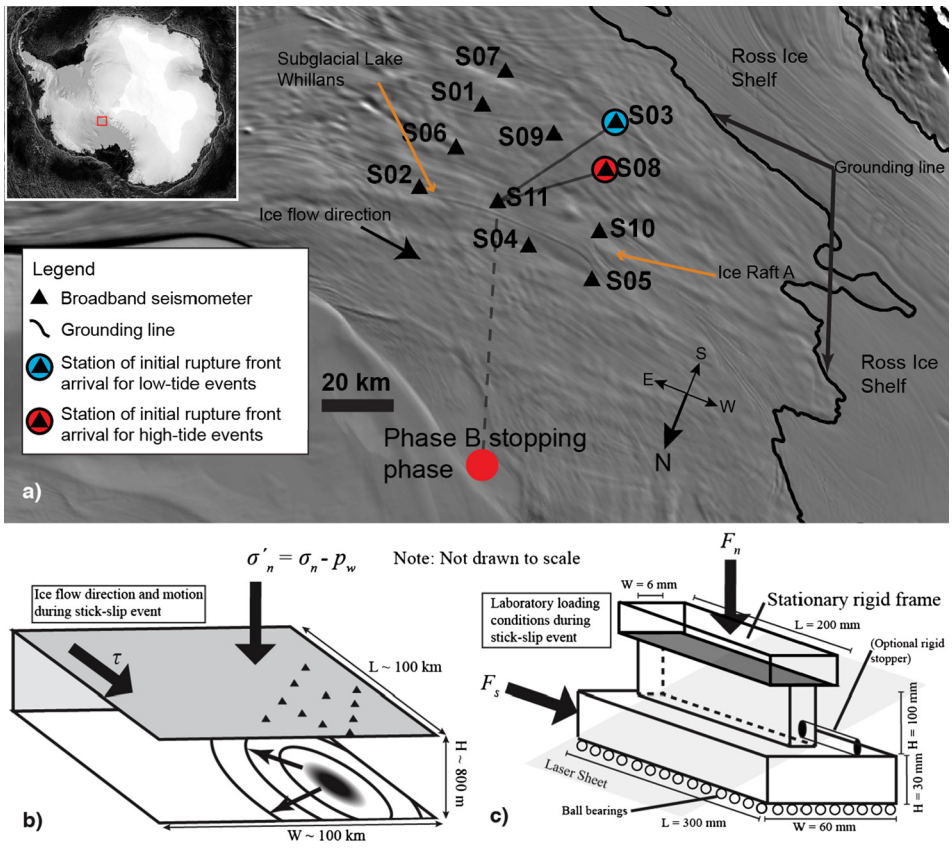

Fig. 1. Whillans Ice Plain location and illustrations of loading conditions. (A) Locations of stations deployed during the 2010 field season and the major geographic features: the grounding line, Ice Raft A and Subglacial Lake Whillans. The rupture front is initially observed at station S03 for low tide events. The rupture front is initially observed at station S08 for high tide events. Solid and dashed lines are used to indicate distances over which rupture speeds are calculated. Grounding line is the Antarctica Surface Accumulation and Ice Discharge (ASAID) grounding line (Bindschadler et al., 2011). Loading configuration prior to slip and propagation of rupture fronts during slip events for the two systems: (B) Whillans Ice Plain bidaily stick-slip events and (C) laboratory measurements of stick-slip at an interface between two poly(methyl-methacrylate) (PMMA) blocks. The optional stopper is used to create spatially nonuniform stresses along the interface (cf. Fig. 5B–C) that are peaked near the stopper. The oblique gray shading indicates light that illuminates the interface for rupture front detection by a high-speed camera.

The systematics of the Whillans Ice Plain system suggests a major role for the variations in tidal loading in controlling the final rupture. In this study, we refine the fundamental observational constraints on the propagation of slow slip at Whillans Ice Plain with new field observations and proceed to construct a laboratory analog model of the slip events that reproduces the fundamental dynamics.

2. Rupture propagation

2.1. Whillans Ice Plain stick-slip

To study the rupture process in detail, we installed an array of 11 broadband seismometers on the Whillans Ice Plain for a period of 1 month during the 2010 field season (Fig. 1). We use this data to locate the initiation points of slip events and measure the mean rupture velocity with a ∼5% reduction in uncertainty (see supplementary material) compared to ours in a slightly different way than was possible with previous study (Walter et al., 2011). The new local seismic data allows us to both track the rupture across the network and to use beamforming to improve the location of the end of the rupture, which is critical to improving the rupture velocity estimates. The new field dataset allows us to draw further conclusions about rupture speed variability between different events and along the rupture path of the WIP.

We estimate the mean rupture velocity by measuring the travel time between the nucleation point and the generator of a distinct barrier phase. The azimuth of the barrier phase relative to the seismic network is determined by finding the direction that focuses the observed radiated energy, i.e., beamforming (Rost and Thomas, 2002). As discussed in the supplementary material, the wave front curvature over the network is negligible and therefore we use a plane wave approximation to determine the backazimuth (supplementary Fig. S2). We then infer a rupture location by projecting the backazimuth to the edge of the ice. Estimates of azimuth indicate a source in the direction of Phase B (Walter et al., 2011) in Fig. 1, with a preferred wave speed consistent with the surface wave speed for the ice sheet in this region. The estimate of the barrier phase location provides a fixed point for rupture propagation and we use this estimate to calculate the mean rupture velocity, similar to previous work (Walter et al., 2011) (see supplementary material).

Loading of the Whillans Ice Plain basal interface varies over time. The tides act as a small-amplitude perturbation the gravitationally-driven flow of the Whillans Ice Plain as it flows into the Ross Ice Shelf (Bindschadler et al., 2003). During our deployment, the location of the initiation point varies with modeled tide. Events that begin at low tide (first arrival at station S03, blue circle in Fig. 1) nucleate closer to the grounding line than those that begin at high tide (first arrival at station S08, red circle in Fig. 1). This pattern in nucleation locations is consistent with most of the observations of Winberry et al. (2011) and Pratt et al. (2014). In this manuscript we use low and high tide events to describe the nucleation of slip events. The tidal height in the Ross Sea is calculated using the model of Padman et al. (2003), where the sign of the vertical tide indicates whether an event initiates at low (negative) or high (positive) tide.

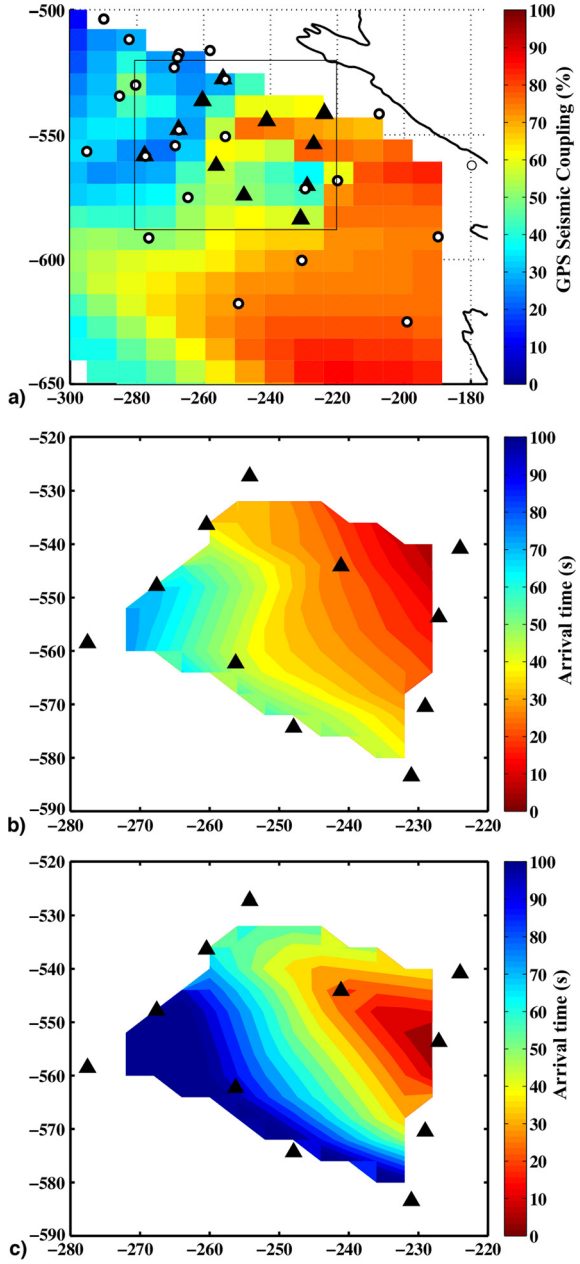

Fig. 2. Inter-event loading and slip event nucleation geometry. Black triangles indicate locations of broadband seismometers. (A) Seismic coupling inferred from the continuous GPS stations (white circles). The local seismic coupling is the total displacement that occurs during the sum of all slip events over a 14-day time period divided by the total displacement that occurs at each GPS station over the same 14-day period. (B) Low-tide event average arrival times and (C) high-tide event average arrival times based on the 2010 field season seismic network (black triangles). Time 0 in both (B) and (C) is the arrival time at the closest station. The contours are interpolated slip front arrivals at the discrete seismic stations. The x- and y-axes of (A–C) represent the South Polar Stereographic grid (km).

Previous studies suggest that basal interface conditions may play a role in the location of the nucleation (Winberry et al., 2009; Pratt et al., 2014). In order to highlight regions of the Whillans Ice Plain where basal coupling may be high, we calculate the seismic coupling on the Whillans Ice Plain in Fig. 2A by computing the fraction of slip that occurs during discrete slip events. We utilize GPS datasets from two separate GPS campaigns collected during an experiment in 2004–2005 (Winberry et al., 2009) and a project investigating subglacial lake activity spanning the years 2007–2012. For each experiment, we choose a single 14-day period when the most stations are operating, and compute the seismic coupling. We define the local seismic coupling at a station as the total displacement that occurs during the slip events over a 14-day period divided by the total displacement that occurs at each GPS station over that time period. This is analogous to the seismic coupling defined for subduction zone faults (Ruff and Kanamori, 1983). For the earlier data (Winberry et al., 2009), we compute the seismic coupling spanning days 332–346 in 2004 and for another experiment, we compute the seismic coupling spanning days 339–353 in 2008. We assume that the temporal variation in coupling is negligible over the 4 years between deployments and that combining 14 days of data effectively averages the coupling ratio over multiple slip events.

Once ruptures nucleate, the events on the Whillans Ice Plain include four major features. First, the mean rupture velocities, V_{mean}, of Fig. 3A are significantly slower (100–240 m/s) than both the shear wave velocity in ice (1900 m/s) (Blankenship et al., 1987) and plausible values of the wave velocity for the underlying sedimentary basins at a scale relevant to rupture propagation (∼800–2800 m/s) (Trey et al., 1999).

Secondly, V_{mean} co-varies with the time since the previous event (Fig. 3A) and slip measured during each event (Fig. 3B). Previous analysis utilized a combination of distant seismic arrivals and/or GPS data to suggest such a relationship (Walter et al., 2011; Winberry et al., 2011). Here we provide an assessment using local seismic data (Fig. 3A). The average rupture speed measurement (see supplementary information) is the estimate of rupture speed over the ∼100 km from nucleation to the barrier phase located downstream (e.g. Pratt et al., 2014; Fig. 1, this paper). This measures the time for the rupture to propagate from nucleation to barrier phase, which is distinct from previous higher estimates for rupture speed closest to the nucleation within the first tens of seconds (e.g. Pratt et al., 2014). The correlation implies that the V_{mean} co-varies with the mean basal shear stress accumulated in the interseismic period up to the time of slip nucleation (Bindschadler et al., 2003; Winberry et al., 2009).

Thirdly, the rupture velocity varies significantly along the rupture path (Fig. 2). This is consistent with observations from 2010 (Pratt et al., 2014). This is most easily seen by examining the high and low tide events separately, where Figs. 2B and 2C indicate that both groups of events rupture at high velocities near the nucleation site. Furthermore, low tide events, which rupture over the same region, rupture at different velocities than high tide events. The relationship between slip event occurrence and tide is shown in Fig. 4A. Pratt et al. (2014) note some exceptions each fortnight where the high tide events nucleated at the grounding line. We note a similar exception (Fig. 4A), where some events occur out of sequence during the fortnightly period when trough to peak amplitudes are small (Fig. 4a inset). During this period, some events nucleate in the low tide location during a positive tide, though they do occur during a trough in the tidal time series. Nonetheless, the majority of the events we observe locate in either high or low tide regions according to tidal amplitude. Fig. 4B shows apparent rupture speed (the rupture speed is apparent because it is calculated along one dimension, between observation points) from either S03 or S08 (depending on low or high tide event) to S11 for a series of events. Slip events that begin at low tide, propagate at much faster speeds towards S11 than high tide events. Within the 2010 seismic network, the low tide events have significantly higher initial rupture speeds, yet slow down quickly to average velocities that are lower than those for high tide events (Fig. 4B). Our measurement of the apparent rupture speed is an estimate of the rupture within the first ∼30–40 km along the ∼100 km rupture path, or the mean “early” apparent rupture speed. The mean early apparent rupture speed indicates faster rupture across the WIP for the low tide events. Early rupture speed differences at the distinct nucleation sites is relatively consistent with previous

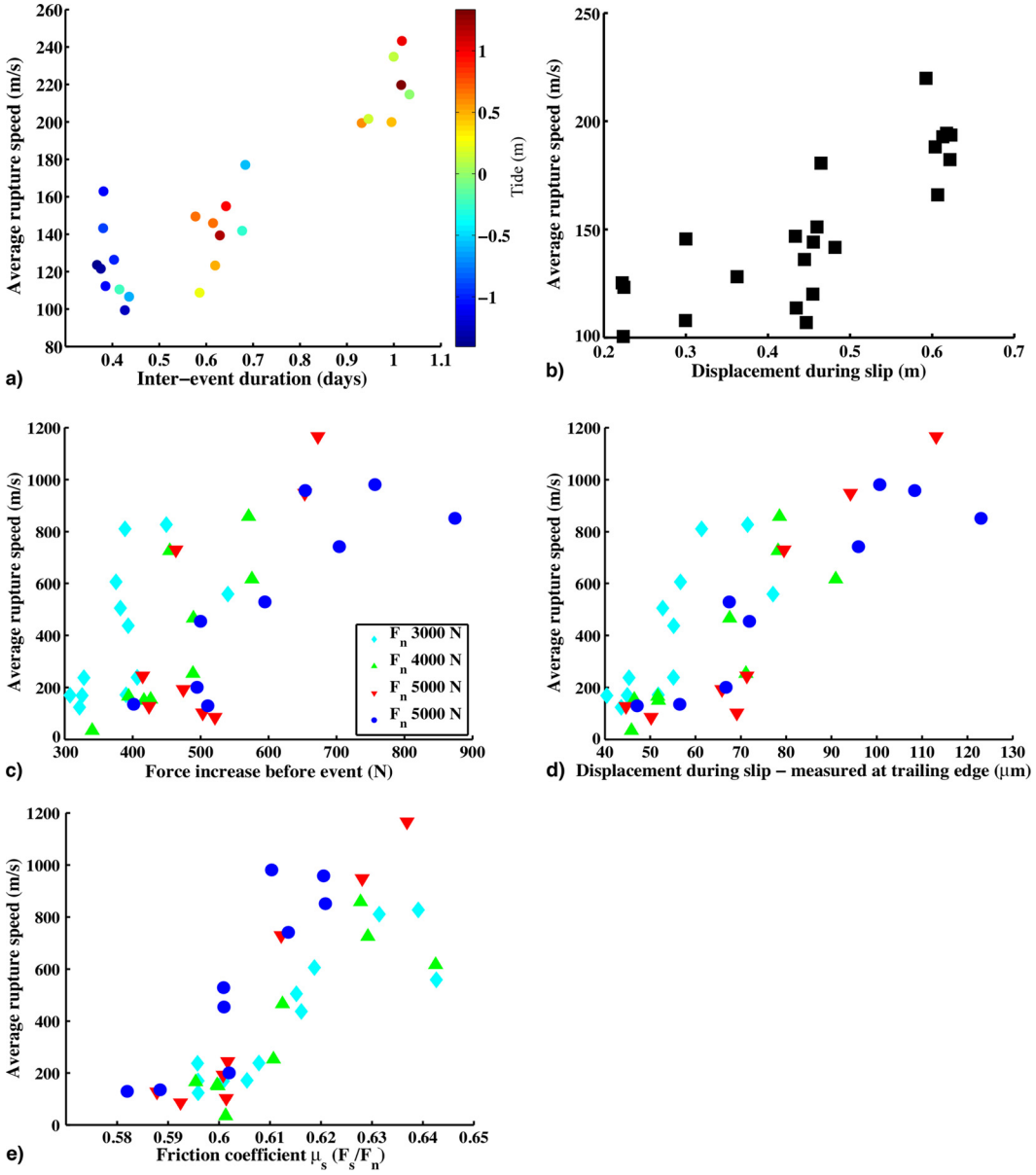

Fig. 3. Average rupture speed estimates over the glacier (A–B) and laboratory (C–E) scales. (A) Co-variation of Whillans Ice Plain average rupture speed with the inter-event duration (recurrence interval). Note that the colors correspond to the tide level at the time of nucleation. (B) Co-variation of Whillans Ice Plain average rupture speed with event displacement, as measured at a GPS station co-located with S10 near the initiation point. (C) PMMA plastic block laboratory average rupture speed co-variation with applied shear force before the event. (D) Co-variation of average rupture speed with laboratory event displacement, measured at the trailing edge of the shear device (E) Average rupture speed as a function of measured ratio $\mu_S = F_S/F_N$ for each event, where both F_S and F_N are the applied shear and normal forces, respectively, measured prior to each event. This normalization by the non-constant effective friction coefficient reduces the scatter. Colors/symbols in C–E are as noted in C and the results in C–E are obtained by the loading described in C *without* the optional stopper.

findings (Pratt et al., 2014); that experiment had stations closer to nucleation and suggest earlier rupture speed estimates of 1 and 1.4 km/s for high and low tide nucleation sites, respectively. Apparent rupture speeds calculated relative to other seismic stations at the edges of our network also exhibit a consistent relationship (Fig. S4) – apparent rupture velocities that are relatively higher for low-tide events.

Fourth, rupture events nucleate in the strongly locked, and therefore highly loaded, regions of the Whillans Ice Plain (Winberry et al., 2009). The spatially interpolated pattern of seismic coupling (Fig. 2A) corresponds directly to the rupture pattern as illustrated by the average arrival times (Figs. 2B, 2C). The seismic coupling maps the inter-event strain field, indicating that areas of high coupling are relatively more loaded at the beginning of the slip event. Slip nucleates in the area with highest loading.

2.2. Laboratory experiments

In the laboratory analog model, we slide one poly(methyl-methacrylate) (PMMA) block past another PMMA block that is held fixed (Fig. 1C). An applied force, F_S, displaces the bottom of the lower block and is gradually increased until a stick-slip event occurs along the 200 × 6 mm interface. Strain gauges at 7–10 points adjacent to the interface locally measure all 2D stress components. In addition, we actively monitor ruptures along the interface by measuring the entire real contact area every 1.7–20 μs. This allows us to track the instantaneous velocity of a typical rupture front as a function of its length together with the temporal evolution of the real contact area as the rupture progresses.

The two transparent poly(methyl-methacrylate) (PMMA) blocks (shear wave speed, $c_S = 1370$ m/s) are pressed together with

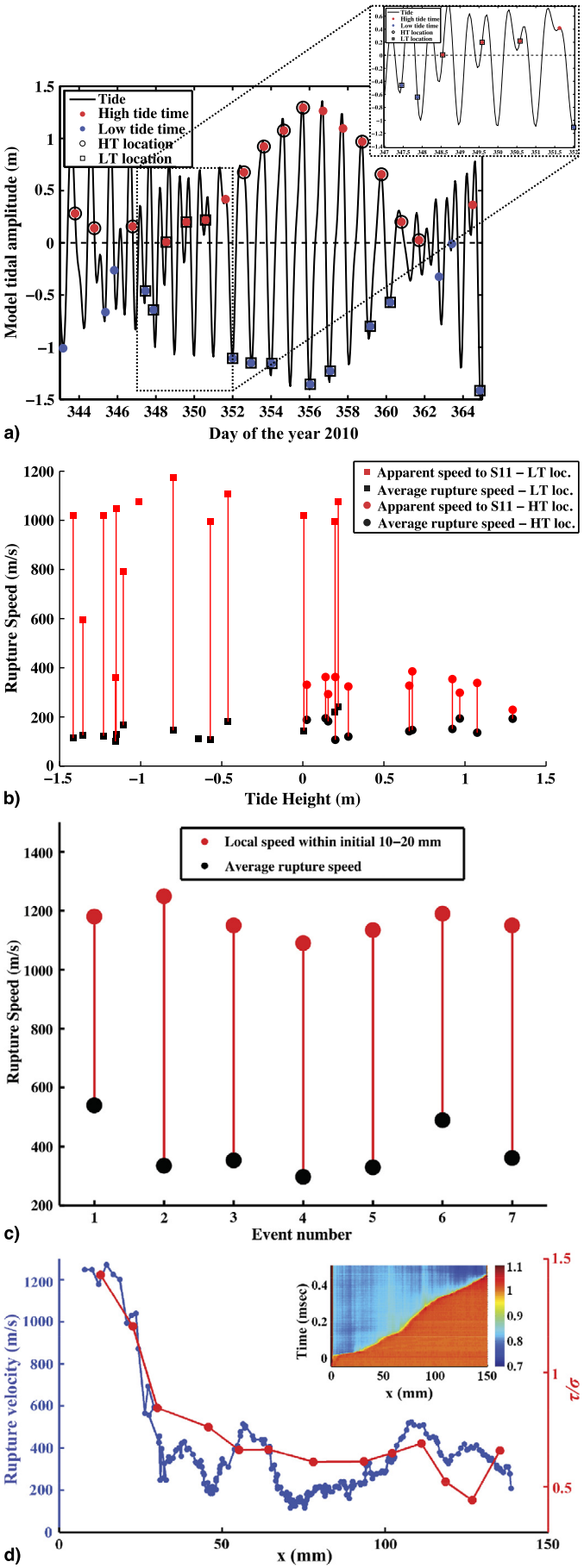

a uniform normal forces F_N that varies between 3000–6000 N. The dimensions of the top (bottom) blocks were $x = 200$, $y = 6$, $z = 100$ mm ($300 \times 60 \times 30$ mm), where x, y, and z are, respectively, the propagation, thickness, and normal loading directions. The contacting faces of the two blocks are first machined to be flat to within 5 μm and then lapped to produce an RMS roughness of approximately 1 μm, thereby forming a rough but uniform contacting surface. The real area of contact is measured with a laser light sheet (see supplementary information).

The bottom block is mounted on a low-friction translational stage constrained to move along the x axis. Once F_N is applied, the shear force, F_S, is applied to the bottom block in the negative x direction via a load cell of stiffness 10^7 N/m at a continuous loading rate of 10–20 N/s. The upper face of the top block is rigidly held in place, so translation of the bottom block imposes elastic stresses on both blocks until rupture takes place along the frictional interface. A rigid stopper is optionally pressed against the leading edge of the upper block, creating a loading effect that locally increases the shear stress in the vicinity of the contact point.

We use the laboratory stick-slip sequences to recreate the four major rupture propagation observations from the field. We perform two sets of experiments (Fig. 1C): uniform application of F_S to the edge of the bottom plate (Fig. 3C), which produces an approximately uniform shear stress along the interface and preferential application of F_S to the leading edge of the top plate (Rubinstein et al., 2007, 2011) (Fig. 1C with stopper), which produces a high stress concentration near the plate edge (Fig. 4D). The uniform shear stress laboratory experiments show a systematic increase of V_{mean} with the inter-event duration (Fig. 3C) and displacement during slip (Fig. 3D). During the leading-edge shear stress laboratory experiments, the non-uniform stress configuration exhibits fast initial rupture near the nucleation, followed by slow rupture further from nucleation. In the next section, we further explore the analogous behavior observed at the two regimes.

3. Discussion

3.1. Laboratory stick-slip reproduces main features of the glacier stick-slip events

We compare the results of the laboratory experiments to the field observations. Firstly, anomalously low V_{mean} occur in the lab (Fig. 3C). Average rupture velocities of as low as 100 m/s are observed. Since the shear wave velocity is 1370 m/s, these correspond to $V/c_s < 0.1$, as observed in nature. An important dis-

Fig. 4. Initial apparent rupture speed, and average rupture speed measurements for each slip event. (A) Tidal amplitude derived from model output (Padman et al., 2003) with timing in the tidal cycle and initiation location. Inset shows complicated neap tide behavior. (B) For each Whillans Ice Plain event, average rupture speed (black) from Fig. 3A is connected by a vertical red line to apparent rupture speed near the nucleation point (red), with tide height at time of slip event initiation on the x-axis and symbol corresponding to approximate location in Fig. 2 (HT – high tide in Fig. 2C and LT – low tide in Fig. 2B). The majority of low tide location events rupture with initial early mean apparent rupture speed that is significantly higher than average rupture speed along the full rupture path. (C) Laboratory measurements of average rupture speed (black) and initial rupture speed (red) when F_S is preferentially applied to the sample edge *with* the optional stopper. The high initial rupture speeds correspond to regions of high local shear/normal stress ratios. (D) A detailed comparison of the rupture velocity to the spatially dependent shear to normal stress ratio (τ/σ) for the second event within the stick-slip sequence described in (C). Note that the shear (τ) and normal (σ) stresses correspond to stresses measured *prior* to the onset of each slip event. (Inset) The real contact area as a function of time and space from which the rupture velocity measurements are derived. Each horizontal line depicts the change in the real contact area along the entire interface in x, after averaging in the thickness (y) dimension. Sequential lines were photographed at 1.7 μs intervals, and all measurements are normalized by the contact area at $t = 0$. For each time $t > 0$, a sharp drop in contact area (color) occurs at the tip of the rupture front. (For interpretation of the references to color in this figure legend, the reader is referred to the web version of this article.)

tinction between the lab and nature is that laboratory slip events that are loaded sufficiently to first slowly elongate to a transition length and, afterwards, rapidly accelerate to velocities that can either approach or exceed the Rayleigh wave speed. The WIP slip events appear never to have sufficient loading to reach this transition length and thus remain at relatively low rupture velocities. This may be due to the differences in effective loading. Since the Whillans Ice Plain is relatively thin in the loading direction the elastic energy released per unit area should be fairly constant, while in the lower aspect ratio laboratory samples the released energy increases with the crack length. As a result, the laboratory samples should be expected to accelerate much more rapidly.

Secondly, the experiments (Fig. 3C) show a systematic increase of V_{mean} with the inter-event duration like the Whillans Ice Plain (Fig. 3A). Since applied F_s is increased at a constant rate in the experiments, inter-event duration has a one-to-one relationship with force increase before each event. We also find that displacement measurements (slip) at the trailing edge of the shear device (Fig. 3D) systematically increase with the V_{mean}.

Thirdly, when applying the non-uniform stress configuration (application of rigid stopper shown in Fig. 1C), we see that the experiments are able to reproduce the observations of fast initial rupture, followed by slow rupture. As shown in Fig. 4C, once nucleation barriers are overcome, ruptures nucleate with high initial velocities that are followed by slow rupture propagation.

Fourthly, the laboratory events with the high leading edge shear stress configuration nucleate at the edge adjacent to the rigid stopper, which is an area of highest shear loading locally. Specifically, the ratio of shear stress to normal stress is highest near the nucleation point (Fig. 4D) and the local rupture velocity co-varies with the local stress ratio. These observations are consistent with both previous similar experiments (Ben-David et al., 2010) and the dependence of the mean rupture velocity with the ratio that was demonstrated in Fig. 3E. As discussed above, the rupture slows as it propagates away from this high stress region.

The two sets of relatively simple frictional laboratory experiments presented in Figs. 3 and 4 capture the various aspects of the Whillans Ice Plain observations, including a rupture velocity that co-varies with the loading conditions and is significantly lower than the shear wave velocity. Two sets, rather than one set, of experiments are needed to highlight the analogy because in the uniform shear stress experiments (Fig. 3), the initial stresses were much more uniformly distributed and wide ranges of values are obtained to compare mean stress and mean rupture velocity. The second experiment, with heterogeneous leading-edge shear stress, produces a wide range of variations in local rupture velocity. Each set of experiments reproduce features of the Whillans Ice Plain on its own, but the data is shown separately to especially highlight certain features of the event ruptures

3.2. Role of loading in determining failure conditions and rupture dynamics

We have established that the model system reproduces the essential features of the natural system: low mean rupture velocity, co-variance between rupture velocity and loading time, decreasing rupture velocity during propagation and nucleation at the site of highest loading.

The most important conclusion from this work is that slow slip events can be created due to frictional failure with no further complicating factors. Homogeneous, solid sliding plastic blocks reproduce the essential features of the Whillans Ice Plain. No more complex model is necessarily required.

We speculate that the success of the simple model for the Whillans Ice Plain stems in part from the relative simplicity of the isolated stick-slip system. Tectonic earthquakes seldom occur in isolation and are constantly influenced by the motion of neighboring faults. In the absence of these complications, a laboratory model closely related to a classical slider-block does an excellent job of reproducing behavior, even for slow-slip events.

A secondary conclusion of this study is that the observed systematic variations in rupture velocities are governed by the applied stresses. The same interface can generate both slow and fast events, depending on stress. This is in contrast to most slow-slip-event modeling studies, which are rather focused on the role of the friction law and imply a dichotomy between slow and fast faults based on frictional differences. In the framework of fracture mechanics, this is an expected result. In fact, recent studies (Svetlizky and Fineberg, 2014) have shown that once interface rupture is initiated, the stress fields surrounding the rupture tip are quantitatively described by the classic fracture mechanic solutions for a propagating shear crack. It is well-established that a crack can propagate at applied stresses, $\Delta\tau$, that are much lower than material yield strengths (e.g., Bonamy, 2009; Lengline et al., 2011). Here, we define $\Delta\tau$ as the difference between the externally applied stress at the time of nucleation and the dynamic stress during failure (e.g. Rice, 1980). All else being equal, the rupture velocity increases with the amount of released elastic energy, which is proportional to $\Delta\tau^2$. Rupture and slip velocities for theoretical cracks do not, necessarily, reach the limiting rupture velocity – especially when the energy released does not rapidly increase with the rupture's length. What determines the applied stress, $\Delta\tau$, for the onset of friction instabilities? The answer lies in the mechanism for rupture nucleation, which is not presently understood (e.g. Ben-David et al., 2010). If the nucleation condition were governed by a material-characteristic static friction coefficient, $\Delta\tau$ would be independent of the tidal loading conditions. The results presented in Fig. 3 suggest that this is not the case and that the applied stress at initiation, $\Delta\tau$, is varying among the events.

In earthquake physics, events where the amount of slip is deterministically controlled by the loading since the last event are termed slip-predictable (Fig. 5; Shimazaki and Nakata, 1980). As shown in the hypothetical illustration (Fig. 5A), the shear stress at failure is variable for slip-predictable earthquakes, whereas the eventual size of the event is controlled by the time between failure (Fig. 5C). Alternatively, in the time-predictable model, the system reaches a constant failure threshold and an event occurs (Fig. 5B), though the size of the event is not known (Fig. 5D). The Whillans Ice Plain behavior over multiple stick-slip cycles is more consistent with a slip-predictable model (Fig. 5E; Fig. S5). The variance is reduced by a factor of 4.8 for the slip-predictable model relative to the time-predictable model (see supplementary information and Fig. S5). Therefore, the shear stress at failure is variable. The question remains: what controls the failure stress and nucleation timing?

Winberry et al. (2009) suggested that the peculiar condition of ice near its melting point could produce a sufficiently rapid (nonlinear) healing process to generate variability in the yield strength of the bed to explain the observations. However, we obtain the same type of rupture variability in the laboratory with a simple PMMA system. Therefore, interevent healing due to a phase transition is not likely the answer.

An alternative possibility is that material heterogeneity on the base allows different regions, with differing frictional thresholds, to be activated as the ice sheet flexes through the tidal cycle (Fig. 2A). Material heterogeneity is an attractive hypothesis as a control on event nucleation (Pratt et al., 2014); however, the laboratory experiments show similar behavior even in the absence of large-scale spatial variability. The continuous variation of rupture speed with force before the event in Fig. 3C demonstrates that material heterogeneity is not required. The variability of the high tide events in

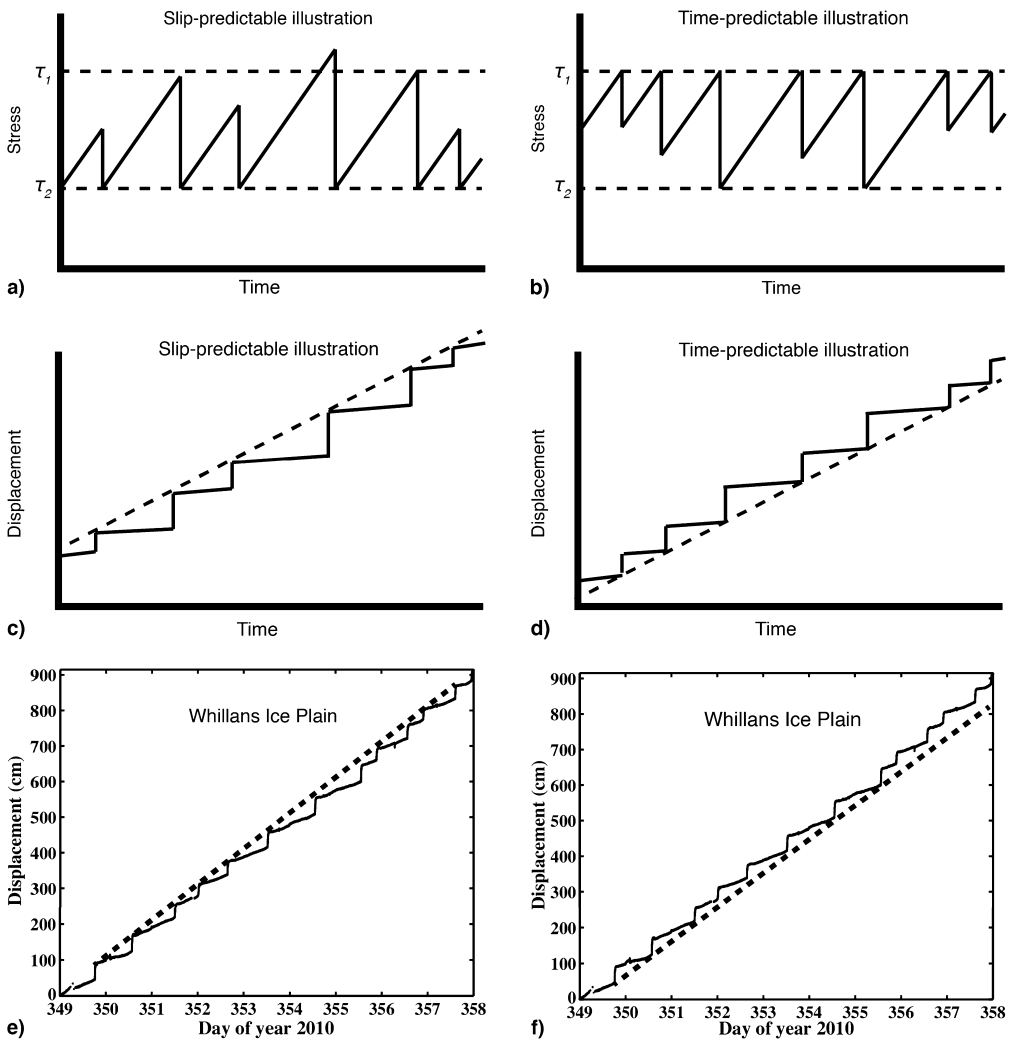

Fig. 5. Schematic illustration of slip-predictable earthquake behavior (adapted from Shimazaki and Nakata, 1980) and observed horizontal displacement for Whillans Ice Plain over multiple slip events. (A) In the slip-predictable model for earthquake occurrence, an event does not occur at a constant threshold shear stress (τ_1). Rather, after each event, the shear stress reduces to a minimum fault stress (τ_2). If shear stress accumulates at a constant rate in between events, then the eventual magnitude of subsequent events can be predicted at any point in time. (B) In the time-predictable model, there is a constant failure threshold (τ_1) where an event occurs when it is reaches the threshold. However, the size of the event cannot be predicted. (C) Illustration of displacement through time shows a slip history that directly reflects the stress drops in (A). (D) Illustration of displacement through time shows a slip history that directly reflects the stress drops in (B). (E) Horizontal displacement from a GPS station co-located with S02 on the Whillans Ice Plain with line drawn to illustrate cumulative displacement after the series of events. (F) Same horizontal displacement record with line drawn to illustrate cumulative displacement prior to slip events. For the 30 days of observation in December 2010, the variance of the linear fit for the slip-predictable model is reduced by a factor of 4.8 relative to the time-predictable model, suggesting that the Whillans Ice Plain is slip-predictable. (See Fig. S5.)

Fig. 3A (inter-event durations ~0.55–1.05 d for similar tide level) also suggests that there is more variability in the natural rupture velocities than can be explained by invoking two different frictional thresholds at the two nucleation sites.

A third possibility is that averaging the stress for failure over the entire interface misses an important aspect of the loading geometry. As the ice sheet (or plastic sheet) flexes, the bed experiences a spatially complex field of concentrations of normal and shear stresses. Recent experiments (Ben-David and Fineberg, 2011; Passelègue et al., 2013) have shown that a constant value for the ratio of applied shear to normal stress on the entire block is a poor predictor of failure. The same result is shown in the current experiments. The coefficient of friction for the entire sample μ_S is defined as the ratio of applied normal force, F_n, to shear force, F_s, as defined in Fig. 1. Fig. 3E shows a variation in μ_S that is much smaller than the nearly 100% variation observed under different loading conditions (Ben-David and Fineberg, 2011; Passelègue et al., 2013), but still resolvable.

Events with a higher average value of μ_S at failure have a higher value of $\Delta\tau$ and therefore are expected to have a higher mean rupture velocity V_{mean}. This expectation is met in the laboratory. The recorded V_{mean} increases with μ_S (a measure of the globally applied stresses) and the data from experiments with different normal stresses collapses to a single trend (compare Fig. 3E to Fig. 3C).

The correspondence between the initially applied stresses and rupture velocity also exists at local scales. At the Whillans Ice Plain grounding line, flexure of the ice sheet may result in localized basal stress concentrations. Local GPS data collected across the grounding line 80 km from the study site during a few days in January 2011 shows that when the ice shelf level goes below the grounding line at low tides, its motion causes an upward flexing of the ice shelf within 5–10 km of the grounding line (Fig. 6). Unfortunately, the deployment is not adjacent to the nucleation points, but does capture the ice flexure across a grounding zone with similar ice thickness to the low tide nucleation area. Upward movement at the forebulge may indicate a normal stress reduction (e.g. Walker et al., 2013), though the normal effective stress is reduced only if the subglacial tills behave at least partially as a drained aquifer.

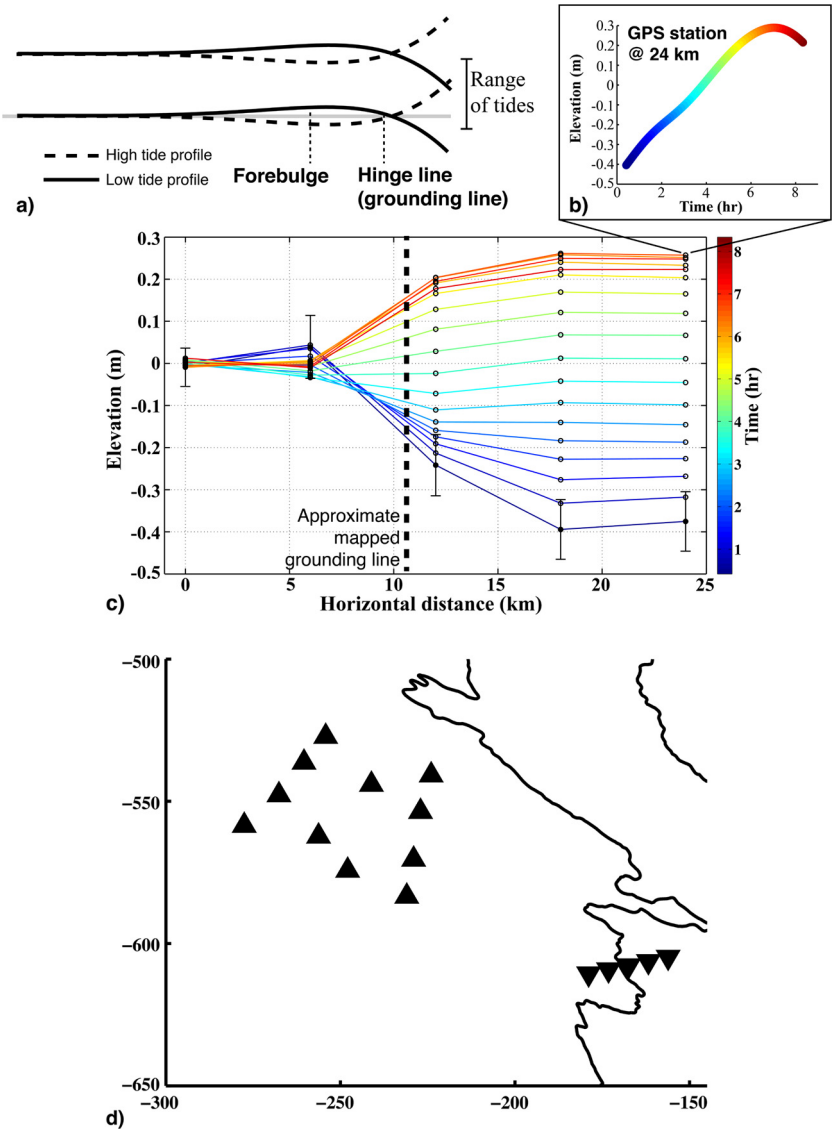

Fig. 6. Flexure along the grounding line on the Whillans Ice Plain. (A) Schematic of flexure cross-section under a line load, including features of the flexure profile. (B) The elevation at the GPS station located at 24 km along the profile. (C) Elevations (with mean removed) of a set of five stations with lines connecting the stations at the same point in time, which demonstrates the flexure geometry across the Whillans Ice Plain grounding line. Vertical errorbars are shown for the first measurement as one standard deviation of vertical position signal, indicating a noisy signal. The average vertical position has been subtracted from the vertical position time series so that all stations plot horizontally on the same line; though there exists a permanent slope across the grounding line (Horgan and Anandakrishnan, 2006). (D) Map outline showing the seismic station (triangles) and the 5 GPS stations (inverted triangles) temporarily deployed across the grounding line that were used to measure (C).

This effect and the estimation that local shear stress at low tide in this region has been estimated to be over 3 times higher than at high tide (Winberry et al., 2011), leads to the expectation that the local shear to normal stress ratio (τ/σ) in the vicinity of the nucleation point should be significantly larger during low tides than at high tides and may explain the fast initial rupture for the low tide events (Fig. 4B). High tide events are not likely influenced by elastic flexure, as they nucleate nearly 30 km from the grounding line. Nucleation during high tides closer to S08 may also be influenced by high hydropotential where less liquid water would be available for lubrication (Winberry et al., 2011), bedrock, or other higher competence material that generate basal asperities, which act to localize strain. While the majority of the events we observe locate in either high or low tide regions according to tidal amplitude, Pratt et al. (2014) report some events over the course of a neap tide that occur out-of-sequence (e.g. grounding line location during a high tide). It is plausible that during neap tides, the interfacial shear stress imparted by flexure near the edge of the Whillans Ice Plain is significantly smaller that the shear stress across the broader region. Nucleation is probably subject to a variety of poorly understood conditions. Though it may occur at whichever location experiences the locally higher shear-to-normal stress ratio and during a neap tide, when flexure is minimal, the location may be subject to variability. Local surficial roughness in the lab samples may influence nucleation, as well, though the influence of this condition is currently being investigated.

A flexural geometry on the Whillans Ice Plain that results in localized high local shear to normal stress ratios (τ/σ) where nucleation occurs during low tides, is in analogy with the laboratory measurements summarized in Fig. 4D. Here, the laboratory events nucleate at the edge of the apparatus, adjacent to the rigid stopper, and the rupture velocity during the event directly corresponds to local value of τ/σ. Thus in both cases, events nucleate in regions where the basal interfacial stresses are higher (local τ/σ), relative to other areas on the frictional surface.

4. Conclusions

The success of the highly idealized system in generating the major features of Whillans Ice Plain slip events suggests a path forward toward understanding the nature of slow slip. A laboratory experiment with no material heterogeneity, complex rheology, or phase changes has recreated the basic observations of slow rupture velocities that depend on loading and local stresses.

The slip-predictable events have a failure condition that varies from event to event depending on the loading conditions. Nucleation of Whillans Ice Plain seismic events occurs during both high and low tides at significantly different stress levels (Bindschadler et al., 2003; Winberry et al., 2009; Walter et al., 2011). This observation complements recent laboratory experiments demonstrating a large range of system-averaged stress ratios over which a frictional system can either be stable or unstable to rupture (Ben-David et al., 2010; Ben-David and Fineberg, 2011). Once nucleation takes place, the rupture speed of stick-slip sliding is controlled by the local stress conditions at the sliding interface, in both the nucleation zone and as the rupture event propagates through other areas.

Frictional processes in fault zones may occur under similar physical conditions, as natural faults have large spatial variations in pre-rupture stress distributions (Lay and Kanamori, 1981). These results imply that loading geometry can have significant effects on resulting rupture dynamics in the absence of any complicating factors.

Acknowledgements

We thank Thorne Lay, Susan Schwartz, and Zhigang Peng for comments on an earlier version of this manuscript and David Heeszel for assistance in the field. Knut Christianson and Huw Horgan assisted in installing the GPS stations at the grounding line. This work was funded primarily by NSF Antarctic Sciences Division Grants 0636970 and 0839142. NASA Earth and Space Science Fellowship (Grant NNX09AO05H) provided support for J.I.W. while at UCSC. J.F. and I.S. acknowledge support of the James S. McDonnell Fund (Grant No. 220020221), the European Research Council (Grant No. 267256), and Israel Science Foundation grant 76/11. We also wish to thank Oded Ben-David for sharing his data and enlightening comments. We thank Paul Winberry for making the GPS data from the 2004 GPS experiment available. Two anonymous reviewers helped improved the manuscript dramatically. The GPS stations were provided by the UNAVCO Facility with support from the National Science Foundation (NSF) and National Aeronautics and Space Administration (NASA) under NSF Cooperative Agreement No. EAR-0735156. Some of the instruments used in the field program were provided by the PASSCAL facility of the Incorporated Research Institutions for Seismology (IRIS) through the PASSCAL Instrument Center at New Mexico Tech. Seismic data collected during this experiment is available through the IRIS Data Management Center. The facilities of the IRIS Consortium are supported by the National Science Foundation under Cooperative Agreement EAR-0552316 and by the Department of Energy National Nuclear Security Administration.

Appendix A. Supplementary material

Supplementary material related to this article can be found online at http://dx.doi.org/10.1016/j.epsl.2014.11.025.

References

Ben-David, O., Cohen, G., Fineberg, J., 2010. The dynamics of the onset of frictional slip. Science 330, 211.

Ben-David, O., Fineberg, J., 2011. Static friction coefficient is not a material constant. Phys. Rev. Lett. 106, 254301.

Beroza, G.C., Ide, S., 2011. Slow earthquakes and nonvolcanic tremor. Annu. Rev. Earth Planet. Sci. 39, 271–296. http://dx.doi.org/10.1146/annurev-earth-040809-152531.

Bindschadler, R.A., King, M.A., Alley, R.B., Anandakrishnan, S., Padman, L., 2003. Tidally controlled stick-slip discharge of a West Antarctic ice stream. Science 301, 1087–1089. http://dx.doi.org/10.1126/science.1087231.

Bindschadler, R., et al., 2011. Getting around Antarctica: new high-resolution mappings of the grounded and freely-floating boundaries of the Antarctic ice sheet created for the international polar year. Cryosphere 5, 569–588. http://dx.doi.org/10.5194/tc-5-569-2011.

Blankenship, D.D., Bentley, C.R., Rooney, S.T., Alley, R.B., 1987. Till beneath Ice Stream B: I. Properties derived from seismic travel times. J. Geophys. Res. 92 (B9), 8903–8911.

Bonamy, D., 2009. Intermittency and roughening in the failure of brittle heterogeneous materials. J. Phys. D, Appl. Phys. 42 (21), 214014. http://dx.doi.org/10.1088/0022-3727/42/21/214014.

Dragert, H., Wang, K., James, T.S., 2001. A silent slip event on the deeper Cascadia subduction interface. Science 292 (5521), 1525–1528. http://dx.doi.org/10.1126/science.1060152.

Horgan, H.J., Anandakrishnan, S., 2006. Static grounding lines and dynamic ice streams: evidence from the Siple Coast, West Antarctica. Geophys. Res. Lett. 33, L18502. http://dx.doi.org/10.1029/2006GL027091.

Kanamori, H., Brodsky, E.E., 2004. The physics of earthquakes. Rep. Prog. Phys. 67, 1429–1496.

Lay, T., Kanamori, 1981. An asperity model of large earthquake sequences. In: Simpson, W., Richards, G. (Eds.), Earthquake Prediction: An International Review. In: Maurice Ewing Ser., vol. 4. AGU, Washington, DC, pp. 579–592.

Lengline, O., et al., 2011. Average crack-front velocity during subcritical fracture propagation in a heterogeneous medium. Phys. Rev. E 84 (3). http://dx.doi.org/10.1103/PhysRevE.84.036104.

Padman, L., Erofeeva, S., Joughin, I., 2003. Tides of the Ross Sea and Ross Ice Shelf cavity. Antarct. Sci. 15 (01), 31–40.

Passelègue, F.X., Schubnel, A., Nielsen, S., Bhat, H.S., Madariaga, R., 2013. From sub-Rayleigh to supershear ruptures during stick-slip experiments on crustal rocks. Science 340, 1208–1211. http://dx.doi.org/10.1126/science.1235637.

Peng, Z., Gomberg, J., 2010. An integrative perspective of coupled seismic and aseismic slow slip phenomena. Nat. Geosci. 3, 599–607. http://dx.doi.org/10.1038/ngeo940.

Pratt, M.J., Winberry, J.P., Wiens, D.A., Anandakrishnan, S., Alley, R.B., 2014. Seismic and geodetic evidence for grounding line control of Whillans Ice Stream stick–slip events. J. Geophys. Res.. http://dx.doi.org/10.1002/2013JF002849.

Rice, J.R., 1980. The mechanics of earthquake rupture. In: Dziewonski, A.M., Boschi, E. (Eds.), Physics of the Earth's Interior. Italian Physical Society and North-Holland Publ. Co., pp. 555–649.

Rost, S., Thomas, C., 2002. Array seismology: methods and applications. Rev. Geophys. 40, 3.

Rubinstein, S.M., Cohen, G., Fineberg, J., 2007. The dynamics of precursors to frictional sliding. Phys. Rev. Lett. 98, 226103.

Rubinstein, S.M., et al., 2011. Slip sequences in laboratory experiments resulting from inhomogeneous shear as analogs of earthquakes associated with a fault edge. Pure Appl. Geophys. 168, 2151–2166.

Ruff, L., Kanamori, H., 1983. Seismic coupling and uncoupling at subduction zones. Tectonophysics 99, 99–117.

Shimazaki, K., Nakata, T., 1980. Time-predictable recurrence model for large earthquakes. Geophys. Res. Lett. 7 (4), 279–282. http://dx.doi.org/10.1029/GL007i004p00279.

Svetlizky, I., Fineberg, J., 2014. Classical shear cracks drive the onset of dry frictional motion. Nature 509, 205.

Trey, H., et al., 1999. Transect across the West Antarctic rift system in the Ross Sea, Antarctica. Tectonophysics 301, 61–74. 1999.

Walker, R.T., et al., 2013. Ice-shelf tidal flexure and subglacial pressure variations. Earth Planet. Sci. Lett. 361, 422–428.

Walter, J.I., Brodsky, E.E., Tulaczyk, S., Schwartz, S.Y., Pettersson, R., 2011. Transient slip events from near-field seismic and geodetic data on a glacier fault, Whillans Ice Plain, West Antarctica. J. Geophys. Res. 116, F01021. http://dx.doi.org/10.1029/2010JF001754.

Wiens, D.A., Anandakrishnan, S., Winberry, J.P., King, M.A., 2008. Simultaneous teleseismic and geodetic observations of the stick-slip motion of an Antarctic ice stream. Nature 453, 770774.

Winberry, J.P., Anandakrishnan, S., Alley, R.B., Bindschadler, R.A., King, M.A., 2009. Basal mechanics of ice streams: insights from the stick-slip motion of Whillans Ice Stream, West Antarctica. J. Geophys. Res. 114, F01016. http://dx.doi.org/10.1029/2008JF001035.

Winberry, J.P., Anandakrishnan, S., Wiens, D.A., Alley, R.B., 2011. Dynamics of ice-stream stick-slip motion. Earth Planet. Sci. Lett. 305, 283–289.